PHYSICAL REVIEW D **77,** 065015 (2008)

Scalar field theory with a nonstandard potential

Sebastian Scheffler
Institut für Kernphysik, Technische Universität Darmstadt, Schlossgartenstr. 9, 64285 Darmstadt, Germany

Ralf Hofmann
Institut für Theoretische Physik, Universität Karlsruhe (TH), Kaiserstr. 12, 76128 Karlsruhe, Germany

Ion-Olimpiu Stamatescu
Institut für Theoretische Physik, Universität Heidelberg, Philosophenweg 16, 69120 Heidelberg, Germany
(Received 19 November 2007; published 13 March 2008)

We study the phase structure of a 4D complex scalar field theory with a potential $V(\Phi) = |\frac{\Lambda^3}{\Phi} - \Lambda\Phi|^2$ at zero and at finite temperature. The model is analyzed by mean-field and Monte Carlo methods. At zero temperature the theory falls in the universality class of the 4D Ising model when varying Λ. The situation is less clear cut for variations with respect to Λ at large temperatures and variations with respect to temperature at a given value of Λ. We observe temperature independence of the mass of the first excitation.

DOI: 10.1103/PhysRevD.77.065015 PACS numbers: 11.10.Lm, 05.50.+q, 11.15.Ha

I. INTRODUCTION

The most striking success of the theory of critical phenomena is its ability to explain the coincidence of critical exponents in physical systems that, at first sight, seem to be vastly different.[1] The behavior in the vicinity of continuous phase transitions can be explained in terms of just a few fundamental properties of the system under consideration: The dimension of spacetime and the symmetries of the associated Lagrangian. As a consequence, the tremendous variety of physical systems exhibiting critical behavior is classified by this universality. It thus is of a certain interest to study the nature of phase transitions in a system whose Lagrangian possesses unusual symmetries. Consider the field theory defined on four-dimensional Euclidean spacetime by the Lagrangian density

$$\mathcal{L}(\Phi, \partial_\nu\Phi) = \tfrac{1}{2}\{(\partial_\mu\Phi^*)(\partial_\mu\Phi) + V(\Phi)\} \qquad (1)$$

where the potential for the complex scalar field Φ is given as

$$V(\Phi) := \left|\frac{\Lambda^3}{\Phi} - \Lambda\Phi\right|^2 = \Lambda^2|\Phi|^2 + \frac{\Lambda^6}{|\Phi|^2} - 2\Lambda^4\frac{(\mathrm{Re}\Phi)^2 - (\mathrm{Im}\Phi)^2}{|\Phi|^2} \qquad (2)$$

with Λ being a constant of dimension mass. This model has been proposed in the framework of a more general effective theory as described in [2–4] and we refer the reader to these papers for details. A contour plot of the potential (2) is shown in Fig. 1. Notice that $V(\Phi)$ is symmetric under both of the following discrete transformations: $\Phi \mapsto -\Phi$ and $\Phi \mapsto \Phi^*$ or, equivalently, $\arg(\Phi) \mapsto \arg(\Phi) + \pi$ and $\arg(\Phi) \mapsto -\arg(\Phi)$. Notice also that the shape of the potential suggests the existence of phase transitions.

In this work we aim at obtaining the following information about the theory defined by the Lagrangian (1): First, we are interested in resolving the phase structure of the model in the parameter Λ and the temperature T. The latter will be introduced by an anisotropic coupling γ in a lattice model. That is, we would like to identify the line in the Λ-γ plane which separates the phase with dynamically broken $\mathbb{Z}_2$-symmetry from the phase where this symmetry is respected by the ground state. Second, we intend to investigate the order of the phase transition and—if a continuous phase transition occurs—to determine its critical exponents. Finally, we also determine the mass of the first excitation at both zero and finite temperature. This is used to relate the bare asymmetry parameter γ to temperature.

The paper is organized as follows. In Sec. II we define the lattice version of the continuum field theory given by

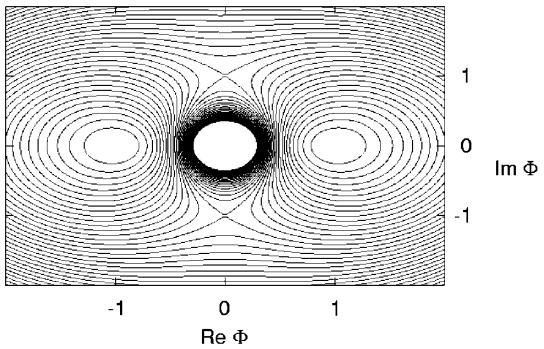

FIG. 1. A contour plot of the potential Eq. (2) for $\Lambda = 1.0$. The axes are scaled in units of Λ. Note the minima at $\Phi = \pm\Lambda$ on the real axis, the saddle points at $\Phi = \pm i\Lambda$ and the pole at $\Phi = 0$.

[1]Confer e.g. [1] for a review on this subject.

the Lagrangian density (1) and discuss the limiting cases $\Lambda \to 0$ and $\Lambda \to \infty$. Subsequently, we carry out a mean-field analysis for the zero temperature case in Sec. III, which allows us to gain first insights into the phase structure of the theory. Section IV is concerned with a Monte Carlo study of the model, and it constitutes the central part of this work. We first design and test suitable Monte Carlo algorithms in Sec. IVA. In the remainder of Sec. IV we obtain the phase diagram, determine the masses and the physical anisotropy, and we carry out a finite-size scaling analysis to determine the critical exponents. Finally, we summarize our results in Sec. V.

II. LATTICE VERSION OF THE MODEL

We discretize the field theory defined by (1) on a four-dimensional lattice in Euclidean spacetime. The field at site n is referred to as Φ_n where n is a lattice point. The lattice spacings along the temporal and spatial axes are denoted by a_τ and a_s, respectively. We label unit vectors by a hat, e.g. $\hat{\tau}$, $\hat{j}$, and their length is one in units of the respective lattice spacing. In particular, $n + \hat{j}$ is the nearest neighbor of site n along the (spatial) j-axis and similarly for $n + \hat{\tau}$. Following common conventions, Roman indices refer to spatial coordinates while Greek indices run over all coordinates of the compactified Euclidean spacetime including the temporal axis. The discretized action then reads

$$S[\Phi] = \frac{a_s^4}{2\gamma}\sum_n \Big\{ -\frac{\gamma^2}{a_s^2}(\Phi_{n+\hat{\tau}}\Phi_n^* + \Phi_n\Phi_{n+\hat{\tau}}^*) - \frac{1}{a_s^2}\sum_j (\Phi_{n+\hat{j}}\Phi_n^* + \Phi_n\Phi_{n+\hat{j}}^*)\frac{2}{a_s^2}(3+\gamma^2)|\Phi_n|^2 + V(\Phi_n)\Big\}. \quad (3)$$

Here we have introduced an asymmetry parameter γ (also referred to as bare anisotropy) between temporal and spatial couplings. This allows us to study the model at finite temperature along similar lines as in [5,6]. We frequently decompose the field variables into their real and imaginary parts according to $\Phi_n \equiv x_n + iy_n$. It will turn out to be convenient to define the following quantities:

$$\Sigma_n := \frac{\gamma}{a_s^2}(\Phi_{n+\hat{\tau}} + \Phi_{n-\hat{\tau}}) + \frac{1}{a_s^2}\sum_j (\Phi_{n+\hat{j}} + \Phi_{n-\hat{j}})$$
$$\kappa := \frac{1}{2}\Big[\Lambda^2 + \frac{2}{a_s^2}(\gamma^2+3)\Big]$$
$$w(x_n, y_n) := -\frac{a_s^4}{\gamma}\Big\{\frac{1}{2}\frac{\Lambda^6}{x_n^2+y_n^2} - \Lambda^4\frac{x_n^2-y_n^2}{x_n^2+y_n^2}\Big\}. \quad (4)$$

At some points it will be convenient to write Φ_n as $\Phi_n \equiv R_n e^{i\Theta_n}$. In terms of these variables the lattice action reads

$$S = \frac{a_s^2}{\gamma}\sum_n \Big\{ -R_n\Big[\gamma^2 R_{n+\hat{\tau}}(\cos\Theta_{n+\hat{\tau}}\cos\Theta_n + \sin\Theta_{n+\hat{\tau}}\sin\Theta_n) + \sum_j R_{n+\hat{j}}(\cos\Theta_{n+\hat{j}}\cos\Theta_n + \sin\Theta_{n+\hat{j}}\sin\Theta_n)\Big] + \Big(3+\gamma^2+\frac{a_s^2\Lambda^2}{2}\Big)R_n^2 + a_s^2\frac{\Lambda^6}{2R_n^2} - a_s^2\Lambda^4\cos(2\Theta_n)\Big\}. \quad (5)$$

Also, we adopt the following notation: For each dimensionful physical quantity (as for instance Φ, Λ etc.) we refer to the corresponding dimensionless quantity as measured in appropriate powers of the spatial lattice spacing a_s by the same symbol endowed with a hat (e.g. $\hat{\Phi}$, $\hat{\Lambda}$ etc.).

Before addressing the dynamics of the model we analyze its behavior in the limits of weak and strong coupling Λ at zero temperature ($\gamma = 1$). For $\Lambda \to 0$ we find

$$S = \sum_n\Big(4 + \frac{\hat{\Lambda}^2}{2}\Big)\hat{R}_n^2 - \sum_{\langle l,n\rangle}\hat{R}_l\hat{R}_n\mathbf{S}_l\cdot\mathbf{S}_n + \mathcal{O}(\hat{\Lambda}^4), \quad (6)$$

where we have defined $\mathbf{S}_n := (\cos\Theta_n, \sin\Theta_n)$. The sum with the subscript $\langle l, n\rangle$ means summation over all pairs of nearest neighbors. This expression resembles the action of a free theory with a mass term.

In the strong coupling limit $\Lambda \to \infty$ all field configurations which do not have the field sitting in one of the two minima of the potential at $\pm\Lambda$ on the real axis are strongly suppressed. The remaining degree of freedom is the sign of the real part of the field, that is $s_n := \mathrm{sign}(\mathrm{Re}\hat{\Phi}_n)$. Its dynamics is governed by lowest-order terms in Λ in the Euclidean action which read

$$S_{\Lambda\to\infty} := -\hat{\Lambda}^2\sum_{\langle l,n\rangle} s_l s_n. \quad (7)$$

Equation (7) is nothing but the familiar Ising model in four dimensions.

III. MEAN-FIELD ANALYSIS

In this section we study the model at hand in the mean-field approximation (MFA). We restrict our analysis to the isotropic case $\gamma = 1$. We find that the relevant symmetry is the $\mathbb{Z}_2$-symmetry relating the real minima of the potential. A phase transition occurs at a critical value $\hat{\Lambda}_C$ of the lattice coupling constant above which this symmetry is dynamically broken. In the following we shall stick to the ''old fashioned'' MFA (see, e.g. [7]) which is more intuitive.

Let us consider the contribution to the overall action of the fixed field variable Φ_n. From Eq. (5) one finds that for $\gamma = 1$ this contribution is given as

$$S(\hat{\Phi}_n) = -\hat{R}_n \sum_{\hat{\mu}} [\cos\Theta_n (\hat{R}_{n+\hat{\mu}} \cos\Theta_{n+\hat{\mu}} + \hat{R}_{n-\hat{\mu}} \cos\Theta_{n-\hat{\mu}}) + \sin\Theta_n (\hat{R}_{n+\hat{\mu}} \sin\Theta_{n+\hat{\mu}} + \hat{R}_{n-\hat{\mu}} \sin\Theta_{n-\hat{\mu}})] + \underbrace{\left(d + \frac{\hat{\Lambda}^2}{2}\right)\hat{R}_n^2 + \frac{\hat{\Lambda}^6}{2\hat{R}_n^2}}_{=:\tilde{V}(\hat{R}_n)} - \hat{\Lambda}^4 \cos(2\Theta_n), \quad (8)$$

where d denotes the dimension. If not stated otherwise we set $d = 4$.

The mean-field approximation amounts to decoupling each field variable $\hat{\Phi}_n$ from its neighbors by replacing each of the $2 \cdot d$ adjacent fields $\hat{\Phi}_{n\pm\hat{\mu}}$ by a mean-field $me^{i\omega}$, thus (dropping the indices "n") Eq. (8) becomes:

$$\begin{aligned} S(\hat{\Phi}) &= -2dm\hat{R}(\cos\Theta\cos\omega + \sin\Theta\sin\omega) - \hat{\Lambda}^4\cos(2\Theta) + \tilde{V}(\hat{R}) \\ &= -2dm\hat{R}\cos(\Theta - \omega) - \hat{\Lambda}^4\cos(2\Theta) + \tilde{V}(\hat{R}). \end{aligned} \quad (9)$$

As a result the partition function factorizes and we only have to deal with a single integral:

$$\begin{aligned} Z(\hat{\Lambda}, m) &= \int d^2\hat{\Phi} e^{-S(\hat{\Phi})} \\ &= \int_0^\infty dR \int_0^{2\pi} d\Theta R \exp\{+2dmR\cos(\Theta - \omega) + \hat{\Lambda}^4\cos(2\Theta) - \tilde{V}(R)\}. \end{aligned} \quad (10)$$

Self-consistency then requires the expectation value of $\hat{\Phi}$ to equal the mean field, hence:

$$\begin{aligned} me^{i\omega} = \langle\hat{\Phi}\rangle &= \frac{1}{Z(\hat{\Lambda}, m)} \int_0^\infty RdR \int_0^{2\pi} d\Theta e^{-S(R,\Theta)} Re^{i\Theta} \\ &=: \varphi(\hat{\Lambda}, m). \end{aligned} \quad (11)$$

This mean-field equation always has the trivial solution $m = \langle\hat{\Phi}\rangle = 0$. It can be shown from the symmetries of the integral that nontrivial solutions require $\omega = 0$ (or π) and $\omega = \frac{\pi}{2}$ (or $-\frac{\pi}{2}$). For small $\hat{\Lambda}$ only the trivial solution $m = 0$ exists. With increasing $\hat{\Lambda}$ a nontrivial solution appears at some value $\hat{\Lambda}_C$, above which $\hat{\Phi}$ develops a nonzero expectation value $m(\hat{\Lambda}) \neq 0$. Since this solution has a smaller free energy than the trivial one[2] it replaces the latter, triggering a phase transition. Some detail is given in the first section of the appendix. It turns out that the solution with $\omega = \frac{\pi}{2}$ sets in at a larger $\hat{\Lambda}$ than the one with $\omega = 0$ and has a larger free energy than the latter, therefore it does not take over. This is physically sensible, since it corresponds to a mean field sitting on the saddle points of the potential and not at the minima. In the following we shall therefore take $\omega = 0$. See also Fig. 2.

[2]The trivial solution has in fact infinite free energy, but this is an artefact of the MFA for a potential singular at 0.

We define

$$F_n(\hat{\Lambda}, m) := \frac{\partial^n Z}{\partial m^n}(\hat{\Lambda}, m) \quad (12)$$

which can be obtained analytically (see the first section of the appendix). Then

$$\varphi(\hat{\Lambda}, m) = \frac{1}{2d}\frac{F_1(\hat{\Lambda}, m)}{F_0(\hat{\Lambda}, m)}. \quad (13)$$

The onset of the symmetry breaking solutions is given by

$$\frac{\partial\varphi}{\partial m}(\hat{\Lambda}_C, 0) = 1. \quad (14)$$

This is displayed in Fig. 2. For later comparison to the Monte Carlo results we quote the numerical value

$$\hat{\Lambda}_{C,\mathrm{MFA}} \simeq 0.2920. \quad (15)$$

It is straightforward to obtain further quantities, for example, the critical exponent β which governs the behavior of the field expectation value near the threshold:

$$\langle\Phi\rangle \sim \left(\frac{\Lambda - \Lambda_C}{\Lambda}\right)^\beta \quad \text{for } \Lambda > \Lambda_C. \quad (16)$$

For this we expand (13) into a Taylor series in m. Making use of relation (12) and noticing that $F_n(\hat{\Lambda}, 0) = 0$ for odd n, we arrive at

$$m = \frac{1}{2d}\frac{mF_2(\hat{\Lambda}, 0) + \frac{1}{6}m^3F_4(\hat{\Lambda}, 0) + \mathcal{O}(m^5)}{F_0(\hat{\Lambda}, 0) + \frac{m^2}{2}F_2(\hat{\Lambda}, 0) + \mathcal{O}(m^4)}. \quad (17)$$

Equating the terms up to fourth order in m one readily finds

$$m^2 = \frac{F_2(\Lambda, 0) - 2dF_0(\Lambda, 0)}{dF_2(\Lambda, 0) - \frac{1}{6}F_4(\Lambda, 0)}. \quad (18)$$

On Fig. 3 we plot the derivative of $\ln(m(\lambda)^2)/2$ as computed from Eq. (18) versus $\ln(\lambda)$ with:

$$\lambda := (\Lambda - \Lambda_C)/\Lambda_C. \quad (19)$$

In the limit $\lambda \to 0$ we obtain $\beta = 0.5$ which is what should

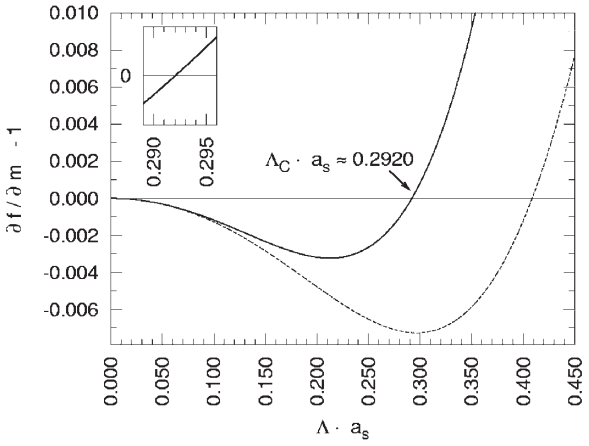

FIG. 2. This figure illustrates the determination of $\hat{\Lambda}_C$ from the criterion $\frac{\partial f}{\partial m}(\hat{\Lambda}, m) - 1 =^! 0$, the inset shows the vicinity of the zero in more detail ($\omega = 0$, solid curve). The dashed curve is the result for $\omega = \frac{\pi}{2}$, showing a later onset.

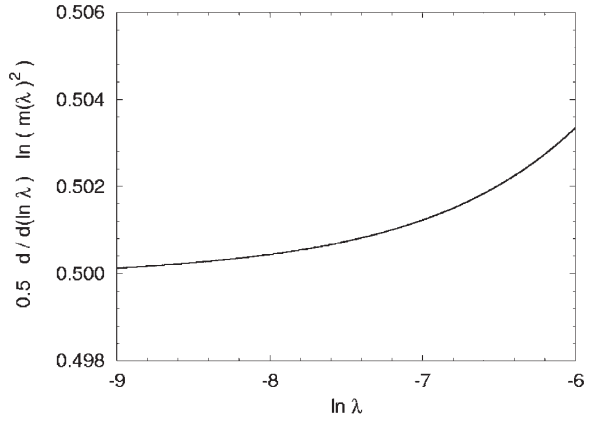

FIG. 3. Determination of the critical exponent β from the MFA. The plot shows $\frac{1}{2}\frac{d}{d(\ln\lambda)}\ln(m(\lambda)^2)$ plotted versus $\ln\lambda$.

be expected for the universality class of the four-dimensional Ising-model.

IV. MONTE CARLO STUDY

In this section we study the model by means of Monte Carlo simulations. We first outline algorithms to sample field configurations and discuss their performance. In Sec. IV B we present a phase diagram of the model. Subsequently, we analyze the mass gap of the theory at zero and finite temperature and estimate the relation between the bare coupling anisotropy γ and the renormalized, physical anisotropy ξ_{aniso} in Sec. IV C. Finally, Sec. IV D presents a finite-size scaling analysis where we determine Λ_C, several critical exponents, and the order of the phase transition.

A. Monte Carlo algorithms for the model

Starting from Eqs. (3) and (4), the contribution to the overall action of a fixed site n can be written as

$$S(\Phi_n) = \frac{\kappa}{\gamma}\left(x_n - \frac{\mathrm{Re}\Sigma_n}{2\kappa}\right)^2 + \frac{\kappa}{\gamma}\left(y_n - \frac{\mathrm{Im}\Sigma_n}{2\kappa}\right)^2 - w(x_n, y_n). \tag{20}$$

That is, the action can be decomposed as

$$S[\Phi] = S(\Phi_n) + (\text{terms independent of}\,\Phi_n). \tag{21}$$

First, we implement a standard local Metropolis algorithm [8]. From Eq. (20) one sees that the probability distribution for a single field variable $\hat{\Phi}_n$ in an otherwise fixed field configuration is given by[3]

$$\begin{aligned} p(\hat{\Phi}_n) &\propto e^{-S(\hat{\Phi}_n)} \\ &\propto \exp\left\{-\frac{\hat{\kappa}}{\gamma}(\hat{x}_n - \hat{x}_0)^2\right\}\exp\left\{-\frac{\hat{\kappa}}{\gamma}(\hat{y}_n - \hat{y}_0)^2\right\} \\ &\quad\times \exp\{\hat{w}(\hat{x}_n, \hat{y}_n)\}. \end{aligned} \tag{22}$$

[3] $w(x, y)$ has been defined in Eq. (4).

A local Metropolis algorithm can be implemented by generating proposals $\hat{x}'$ and $\hat{y}'$ for the new real and imaginary part of $\hat{\Phi}_n$ from Gaussian distributions with the parameters found in Eq. (22). The trial field variable $\hat{\Phi}'_n \equiv \hat{x}' + i\hat{y}'$ is accepted with probability $\min\{1, \exp[\hat{w}(\hat{x}', \hat{y}') - \hat{w}(\hat{x}_n, \hat{y}_n)]\}$. We shall refer to this algorithm as *M-G* in the following. A different way to set up a local Metropolis sampler is to generate trial variables $\hat{x}'$ and $\hat{y}'$ from a homogeneous distribution on the intervals $[\hat{x}_0 - a_x, \hat{x}_0 + a_x]$ and $[\hat{y}_0 - a_y, \hat{y}_0 + a_y]$, respectively. Here a_x and a_y are constants which can be chosen arbitrarily. Given the proposal $\hat{\Phi}'_n = \hat{x}' + i\hat{y}'$ one then accepts $\hat{\Phi}'$ with the probability $\min\{1, \exp[S_E(\hat{\Phi}_n) - S_E(\hat{\Phi}')]\}$. We dub this procedure *M-h*. The efficiency of this algorithm will strongly depend on the choice of the interval widths a_x and a_y.

It is expected that the algorithm *M-h* can be rendered more efficient by implementing it as "modified Metropolis algorithm" [9] which performs several subsequent updates of the same site during each sweep over the lattice. We will test this procedure as well and refer to it as *M-m*.

Since we anticipate the occurrence of a continuous phase transition (cf. Sec. III) we also implement a Cluster algorithm in order to reduce the possible impact of critical slowing down. We adapt the methods discussed in [10,11] to our model. Our implementation of the cluster algorithm is outlined in detail in the appendix Sec. 2. Given that the cluster algorithm only refreshes a subset of the degrees of freedom it has to be combined with one of the local Metropolis samplers described in the beginning of this section. We have chosen the algorithm *M-G* for this purpose and we refer to this combination of the cluster algorithm and *M-G* as *CA* in the following.

We now report on our practical experiences with the above algorithms. In order to compare the algorithms we have carried out simulations using each of the algorithms on a 12^4-lattice at fixed $\hat{\Lambda} = 0.5$ varying the coupling anisotropy γ. After initializing the lattice in a disordered way ("hot start") 20 000 thermalization sweeps were performed and 1000 configurations were subsequently analyzed, separated by 50 sweeps each. We have computed the expectation value of the field's modulus[4] $\langle|\hat{\Phi}|\rangle := |\sum_n \hat{\Phi}_n|/V_4$ and the corresponding susceptibility $\hat{\chi} = V_4[\langle|\hat{\Phi}|^2\rangle - \langle|\hat{\Phi}|\rangle^2]$ (V_4 denotes the four-dimensional volume of the lattice.). The results are displayed in Fig. 4. As can be seen, there is a phase transition at $\gamma \simeq 14$ (This will be discussed in detail in Sec. IV B.) Below this transition ($\gamma \lesssim 12$) the results obtained with all algorithms agree within the margins of error.[5] However, deviations exist for larger values of γ. We think that these are due to inefficiencies of some of the algorithms in the vicinity of the phase transition. The *M-h* update performs particularly

[4] Cf. [12] for a discussion of the validity of this procedure and its systematic errors.

[5] These were estimated by means of the jackknife method.

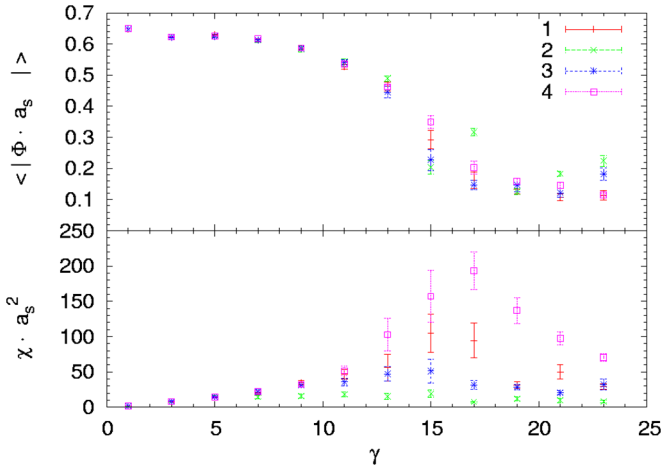

FIG. 4 (color online). Plots of the order parameter and the susceptibility as obtained using the algorithms discussed in the text. The numbers in the legend are related to the algorithms in the following way: (1) *M-G*; (2) *M-h* (3) *M-m*; (4) *CA*.

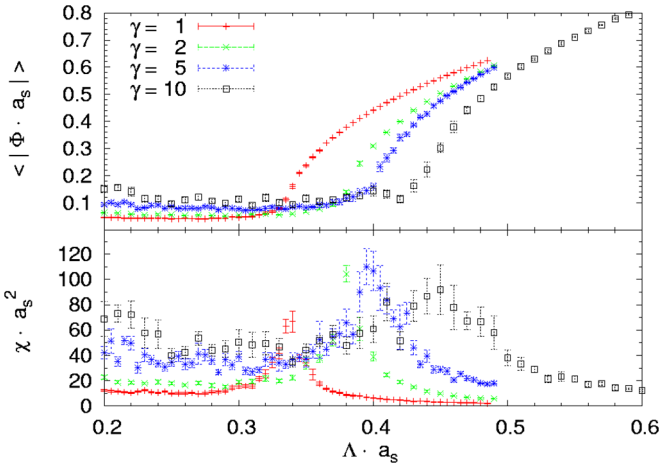

FIG. 5 (color online). Resolving the phase structure by running simulations cutting through the $(\gamma, \hat{\Lambda})$-plane. This figure presents results obtained at fixed values of γ.

poorly in this range. The acceptance rate was very low and this could not be significantly improved by tuning the widths a_x and a_y of the proposal distribution. Its modified version *M-m* performs significantly better; indeed the data is in better agreement with the data generated by means of the other algorithms. We have decided to use the algorithms *M-G* and *CA* exclusively in the remainder of the work because they perform better and do not require tuning the widths of the proposal distributions. We close this section by briefly describing some other technical details. In Table I an overview is given on the statistics and algorithms used to obtain the results quoted in this work. Here, n_{thermal} denotes the number of thermalization sweeps that were carried out before observables were measured the first time after initializing the lattice. n_{sweeps} stands for the number of updates of the entire lattice carried out between every two successive measurements. n_{config} gives the number of configurations from which observables were calculated. We have tested ordered, disordered, and mixed phase initial configurations and checked that they yield the same results. We have always applied periodic boundary conditions. The margins of error quoted in this work and displayed in the figures were obtained by means of the jackknife method if not stated otherwise.

B. Phase diagram of the theory

In this section we present a phase diagram of the model in the plane spanned by the parameters $\hat{\Lambda}$ and γ. From the mean-field analysis (cf. Sec. III) we expect spontaneous symmetry breaking to occur within a certain range of this plane.

The phase structure is resolved by running simulations varying one of the parameters while keeping the other one fixed. Figure 5 shows results for the expectation value of the field (i.e. the order parameter for the system under consideration) and the susceptibility as obtained from simulations where the coupling $\hat{\Lambda}$ was increased at different values of the anisotropy parameter γ. The sudden increase in each of the curves displayed in the upper panel together with the simultaneous peak in the susceptibility provides strong indication for a phase transition. Given that the results for the order parameter $\hat{\Phi}$ appear to be continuous we suppose that the phase tran-

TABLE I. Summary of the statistics of the simulations in this work. Confer the text for further explanations.

data displayed/quoted in	n_{thermal}	n_{sweeps}	n_{config}	MC-alg.
Figure 4	20 000	50	1000	various ones
Sec. IV B	10 000 to 20 000	50	1000	*M-G*
Table II	200 000 to 30 000	50	2800 to 200 000[a]	*M-G*
Table III	20 000 to 30 000	50	8000 to 60 000[a]	*M-G*
Table IV	10 000	50	10 000 ($\gamma = 2$), 20 000 ($\gamma = 3$)	*M-G*
Sec. IV D	10 000	50	1000	*M-G*

[a]The number of configurations depends on the lattice size.

sitions are continuous.[6] From the peaks of the susceptibilities we have read off the critical values of the parameters and estimated their errors from the width of the peaks. Plotting the phase transition points in the $(\gamma, \hat{\Lambda})$- plane yields Fig. 6 which provides the phase diagram of the model. Briefly summarizing its content in words, one can say that there is a line of presumably second-order phase transitions separating the symmetric phase at small $\hat{\Lambda}$ and/or high γ from a symmetry broken phase which exists at larger values of $\hat{\Lambda}$ and not too high values of γ. Two features deserve to be commented on. First, it appears as if there is a critical $\hat{\Lambda}_C$ below which spontaneous symmetry breaking never occurs. This can be inferred from the results of the simulations keeping $\gamma = 1.0$ fixed.[7] Second, the numerical value of this critical coupling can be roughly estimated as $\hat{\Lambda}_C \approx 0.3$ which agrees remarkably well with the prediction from the mean-field analysis quoted in Eq. (15).[8] We notice that there are larger errors at high γ. This will be discussed in Sec. V.

We briefly comment on the role of the parameter $\Lambda = \hat{\Lambda} \cdot a_s^{-1}$ which has the dimension of a mass. When investigating the phase structure of the lattice model we consider the dimensionless $\hat{\Lambda}$ as the relevant parameter. On the other hand, we can understand Λ as a cutoff that is externally given. By virtue of the relation between Λ and $\hat{\Lambda}$ we can then interpret a_s as the spatial resolution or, equivalently, a_s^{-1} as a momentum cutoff.

C. Mass gap and physical anisotropy

In this section we determine the mass gap of the theory at both zero and finite temperature and analyze the dependence of the physical anisotropy ξ_{aniso} on the corresponding input parameter γ. First, we study the mass gap of the theory at zero temperature, i. e. on isotropic lattices where $N_\tau = N_x$ and $\gamma = 1$. Before presenting our Monte Carlo results we provide an estimate for the mass from the second derivative of the potential at its minima. Keeping in mind that there is a factor $1/2$ in front of $V(\Phi)$ in Eq. (1) the estimate for the mass at tree level is

$$m_0 = \sqrt{\frac{1}{2}\frac{\partial^2 V}{\partial(\mathrm{Re}\Phi)^2}} = \sqrt{\frac{1}{2}\frac{\partial^2 V}{\partial(\mathrm{Im}\Phi)^2}} = 2\Lambda. \tag{23}$$

This will serve for later comparison to the numerical results. Notice that m_0 is associated with the mass of topologically trivial fluctuations of the field Φ about the minima $\Phi_{\text{min}} = \pm\Lambda$ of its potential. The fact that m_0 is larger than $|\Phi_{\text{min}}|$ implies that these fluctuations do not take place. We have numerically determined the lowest mass of an intermediate state by measuring effective masses computed from time slice correlators. It proved beneficial to run the calculations on lattices with different linear extensions because this allows to find a reasonable trade-off between systematic errors (due to too short a time axis) and statistical errors (due to limited computer time when simulating larger volumes). Table II presents the results for different choices of the coupling $\hat{\Lambda}$.

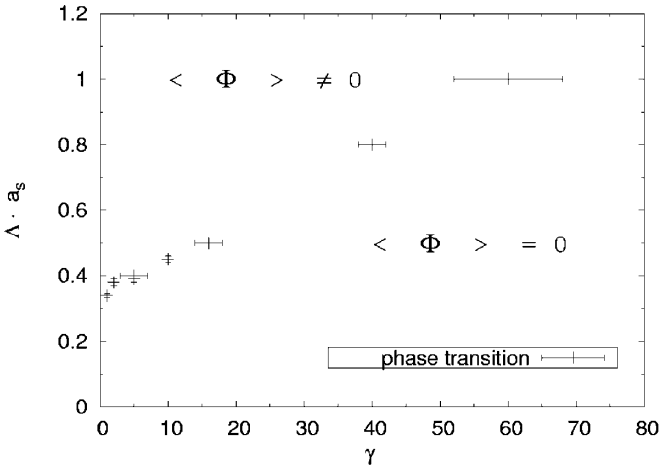

FIG. 6. Phase diagram of the model.

In the next passage we present estimates for the physical anisotropy $\xi_{\text{aniso}} \equiv a_s/a_\tau$ resulting from a given bare anisotropic coupling γ. To this end, we proceed as follows. We require that the physical correlation length ξ be the same when measured along temporal and spatial axes. That is,

$$\xi = a_s \xi_s \stackrel{!}{=} a_\tau \xi_\tau \tag{24}$$

which implies

$$\xi_{\text{aniso}} = \frac{a_s}{a_\tau} = \frac{\xi_\tau}{\xi_s} = \frac{m_\tau}{m_s} \tag{37}$$

where we have used $\xi_s = 1/m_s$ (and, respectively, for ξ_τ) in the last equality. m_s and m_τ denote the masses measured

TABLE II. Results for the masses at zero temperature, i.e. $\gamma = 1$. The last column gives the tree level estimates in units of a_s^{-1} as computed from Eq. (23).

$\hat{\Lambda}$	Lattice	$m[a_s^{-1}]$	Equation (23)
0.5	8^4	0.576 (2)	1.0
0.5	12^4	0.558 (7)	1.0
0.5	16^4	0.554 (6)	1.0
0.8	8^4	1.139 (11)	1.6
1.0	8^4	1.55 (3)	2.0
1.0	12^4	1.57 (6)	2.0

[6]We will provide evidence for the continuous character of the phase transition at $\gamma = 1$ and $\gamma = 10$ in Sec. IV D where we carry out a finite-size scaling analysis.

[7]Physically, we interpret the case $\gamma = 1$ as the zero temperature limit while higher numerical values correspond to nonzero temperature. Thus we consider 1.0 as the lowest attainable value of γ.

[8]Also this issue is addressed in more detail in Sec. IV D.

TABLE III. Results for the physical anisotropy. d in the fifth column denotes the separation at which the effective mass has been evaluated.

$\hat{\Lambda}$	N_x	N_τ	γ	$d[a_s]$	ξ_{aniso}
0.5	12	24	2.0	2	2.01 (4)
				3	1.92 (4)
				4	2.10 (11)
				5	2.2 (2)
				6	2.1 (3)
0.5	8	24	3.0	2	2.98 (2)
				3	2.98 (4)
				4	3.00 (4)
0.8	12	24	2.0	2	1.97 (2)
				3	1.90 (13)
				4	1.8 (4)
0.8	8	24	3.0	2	2.88 (4)
				3	2.90 (12)
				4	3.2 (3)
1.0	8	16	2.0	2	1.88 (8)
				3	2.0 (2)
				4	1.4 (2)
1.0	8	24	3.0	2	2.70 (6)
				3	2.5 (2)
				4	5 (4)

along the respective axis in units of the inverse lattice spacing. We now make the assumption that $\xi_{\text{aniso}}/\gamma = \mathcal{O}(1)$. This was found to hold in the case of ϕ^4-theory [13]. Under this assumption the lattice is approximately isotropic when the edge lengths are chosen as $N_\tau = \gamma N_x$. This choice of the lattice extensions ensures that the impact of undesired finite temperature effects can be neglected. Using such a setup, we have measured effective masses as a function of distance and we have estimated ξ_{aniso} from

$$\xi_{\text{aniso}} \simeq \frac{m_s(d)}{m_\tau(\gamma d)}. \tag{38}$$

The purpose of evaluating m_τ at separation γd is to ensure that the contributions of higher excitations have decayed away to the same extent when comparing the two effective masses. Table III summarizes our results from this procedure. As can be seen there, the physical anisotropy ξ_{aniso} agrees with γ within the margin of error. In particular, this implies for the temperature[9] $T = \xi_{\text{aniso}}/(a_s N_\tau) = \gamma/(a_s N_\tau)$. This shows that γ is related to the physical temperature in a straightforward way and therefore it *a posteriori* justifies our use of γ as a parameter in the phase diagram in Sec. IV B. It has to be noted though that we have only checked the relation between ξ_{aniso} and γ for $\gamma \leq 3$. We assume that we can extrapolate these results to larger values of γ.

[9]We work in units where $k_B = 1$.

TABLE IV. Results for the masses at finite temperature.

$\hat{\Lambda}$	γ	N_x	N_τ	$T[a_s^{-1}]$	$m[a_s^{-1}]$
0.5	2.0	12	12	1/6	0.53 (2)
0.5	3.0	12	12	1/4	0.53 (2)

Finally, we have studied the temperature dependence of the mass. To this end, we have applied the same procedure as in the zero temperature case but this time running the simulation on an anisotropic lattice with $\gamma > 1$. The results are displayed in Table IV. By comparing this result to the corresponding one in Table II one sees that the mass has slightly dropped but in general it does not exhibit a strong temperature dependence.

D. Finite-size scaling analysis for the susceptibility

In this section we carry out a finite-size scaling analysis of the Monte Carlo data for the susceptibility $\hat{\chi}$. This will enable us to determine several critical exponents and hence the universality class of the model. Furthermore, we confirm that the phase transition when varying $\hat{\Lambda}$ at fixed temperature is indeed continuous. The data underlying the discussion in this section have been obtained from simulations on lattices of various linear extensions L. We have varied the coupling $\hat{\Lambda}$ at several choices[10] of γ_{aniso}. In analogy to the definition of a reduced temperature we define a reduced coupling λ as

$$\lambda := \frac{\Lambda - \Lambda_C}{\Lambda_C} \tag{27}$$

where Λ_C denotes the (*a priori* unknown) critical coupling.[11] We denote the correlation length in the infinite volume limit by ξ. Then, the standard finite-size scaling approach states that the susceptibility $\chi_L(\lambda)$ as measured on a finite box of linear extension L is given by

$$\chi_L(\lambda) = \xi^{\gamma/\nu} \chi_0(L/\xi). \tag{28}$$

Here, γ and ν denote the critical exponents such that in the thermodynamic limit $\chi \sim \lambda^{-\gamma}$ and $\xi \sim \lambda^{-\nu}$ in the vicinity of the critical point at $\lambda = 0$. χ_0 is a continuous function which only depends on the ratio L/ξ. Substituting the asymptotic behavior of ξ into the last equation and making the ansatz

$$\chi_0(L\lambda^\nu) \equiv \left(\frac{L}{\xi}\right)^{\gamma/\nu} f(L^{1/\nu}\lambda) \tag{29}$$

[10]Deviating from our conventions in the rest of this work we will denote the bare anisotropy parameter by γ_{aniso} in Sec. IV D in order to avoid confusion with the critical exponent γ.

[11]In fact, we should write this as $\Lambda_C(\gamma_{\text{aniso}})$ since we study the model at various, fixed choices of γ_{aniso}. However, we will suppress the γ_{aniso}-dependence in our notation for the sake of brevity.

TABLE V. Results for $\hat{\Lambda}_C$ and the critical exponents γ and ν at several values of γ_{aniso} as obtained from the finite-size scaling method. The last column gives the value of χ^2 per degree of freedom. The margins of error are the estimates as obtained from the standard χ^2- fit. Confer the text for a comment on systematic errors.

γ_{aniso}	number of data points	$\hat{\Lambda}_C$	γ	ν	χ^2/d.o.f.
1.0	51	0.3299 (3)	0.98 (3)	0.50 (2)	2.2
2.0	140	0.3719 (3)	0.924 (13)	0.449 (11)	1.7
5.0	124	0.3810 (7)	0.84 (3)	0.421 (14)	1.6
10.0	103	0.352 (7)	1.05 (6)	0.67 (5)	1.2

with some continuous function f one arrives at

$$\chi_L(\lambda) = L^{\gamma/\nu} f(L^{1/\nu}\lambda). \tag{30}$$

Assuming an expression for f one can fit data from lattices of different lengths using the last equation and thus one can determine the critical exponents and $\hat{\Lambda}_C$ [The dependence of Eq. (30) on $\hat{\Lambda}_C$ enters via the definition of λ in Eq. (27).]. Introducing a set of six fit parameters a_0 to a_5 our ansatz for fitting f reads

$$y(\hat{\Lambda}, L) := L^{a_1/a_2} \frac{a_3}{\sqrt{1 + a_4^2[L^{1/a_2}(\frac{\hat{\Lambda}}{a_0} - 1) - a_5]^2}}. \tag{31}$$

The significance of the fit parameters is as follows. a_0 corresponds to the value of the critical coupling $\hat{\Lambda}_C$, a_1 and a_2 correspond to the critical exponents γ and ν, respectively. a_5 serves to take into account that the peak of the susceptibility as measured on a finite volume occurs slightly shifted away from its position at $\lambda = 0$ in the thermodynamic limit. The parameters a_3 and a_4 are not of any immediate physical significance but serve to parameterize the function which resembles a Lorentz curve. Table V summarizes the results from fitting our Monte Carlo data while Fig. 7 visualizes the outcome of the finite-size scaling procedure for $\gamma = 1$ and $\gamma = 10$. Several things need to be commented on. First, the margins of error quoted in Table V are the statistical errors obtained from the χ^2-fit[12] in the common way; they appear to be underestimated, in particular, for $\hat{\Lambda}_C$. We think that there are systematic errors that have not been taken into account in Table V which affect the fit. This is because the statistical errors of the Monte Carlo data are largest in the vicinity of the critical point where the finite-size scaling method should make the curves collapse. Therefore, the χ^2-fit gives a lower weight to the data that are more relevant for physical reasons. It is difficult to estimate the numerical size of this effect. Comparing the quality of the fit at the different values of γ_{aniso} [cf. Fig. 7], one sees that it works better at smaller γ_{aniso}. In the limit of high temperature [Fig. 7(b)] the statistical errors are significantly larger. In particular, we think that one should be a bit careful about the estimate for $\hat{\Lambda}_C(\gamma_{\text{aniso}} = 10) \approx 0.35$ which appears unreliable when compared to the value read off from Fig. 5. Giving an interpretation of these results, we first note that the critical exponents γ and ν obtained at $\gamma_{\text{aniso}} \lesssim 2$ agree well with the ones for the Ising model in

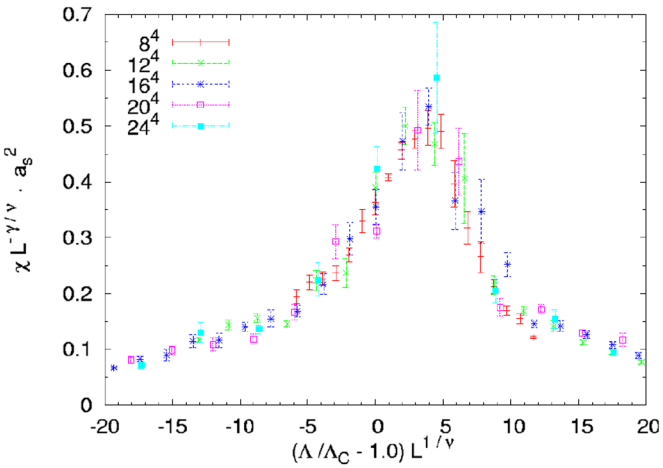

(a) $\gamma_{\text{aniso}} = 1.0$

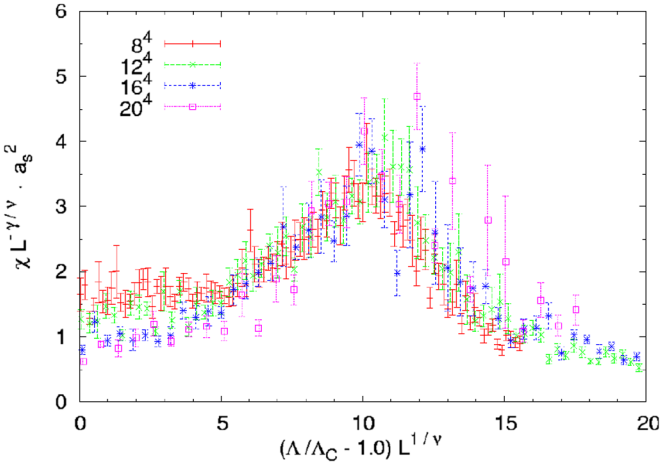

(b) $\gamma_{\text{aniso}} = 10.0$

FIG. 7 (color online). Test of the finite-size scaling. The values inserted for $\hat{\Lambda}_C$, γ, and ν are the ones quoted in Table V.

[12] χ^2 is the common merit function of the χ^2-fit and not the square of the susceptibility χ. Since there should be no risk of confusion we do not introduce an extra piece of notation to distinguish the two quantities.

four dimensions. Thus we deduce that the model lies in the same universality class as the 4D Ising model for these choices of the parameters. At this point it is necessary to discuss the nonrenormalizability of the potential (2). From an expansion about one of its minima[13] one finds that the potential contains contributions up to arbitrary order in the real and imaginary part of Φ. The corresponding coupling constant for a contribution of order n is proportional to $\Lambda^{-(n-4)}$. The terms with a coupling of negative mass dimension are irrelevant for the critical properties of the model [1]. The only relevant and marginal contributions are the terms of order Φ^2, Φ^3, and Φ^4 and the critical exponents should be completely determined by them. The data at higher temperatures is not interpreted in as straightforward a way. From Table V one sees that the critical exponent ν shows a noticeable increase when γ_{aniso} is raised to $\gamma_{\text{aniso}} = 10$ after dropping at intermediate values. In the limit of high temperature (i.e. $\gamma_{\text{aniso}} = 10$), the numerical value of ν is compatible with the corresponding critical exponent of the three dimensional Ising model whose value is 0.630 ± 0.0015 [14]. This observation might hint at the dimensional reduction of the four-dimensional field theory to a three dimensional one in the limit of infinite temperature (or equivalently $\gamma_{\text{aniso}} \to \infty$). Indeed, it was found in [15–18] that a dimensional crossover can be observed in the critical properties of a field theory when the temperature is increased from $T = 0$ towards $T \to \infty$.

From the values quoted in Table V we also infer that the phase transition is always a continuous one. For a first-order phase transition the susceptibility at the critical point diverges proportional to the volume [19–21]. From Eq. (30) it follows that $\chi \sim (L/\xi)^{\gamma/\nu}$. Given that our data is certainly incompatible with $\gamma/\nu = 3$ for all values of γ_{aniso} under consideration we can exclude that the phase transition is of first order.

It is also interesting to numerically determine the exponent β which is defined by Eq. (16) and which has previously been estimated in the mean-field approximation (see Fig. 2). The result of a linear fit to $\ln\langle\hat{\Phi}\rangle$ plotted versus $\ln\lambda$ at $\gamma_{\text{aniso}} = 1$ is shown in Fig. 8. We have only fitted the data from the 24^4-lattice because it provides the best realization of the thermodynamic limit among the available simulation results. The fit yields

$$\beta = 0.453 \pm 0.002 \tag{32}$$

where the error estimate gives the statistical error as computed from a χ^2-fit again. This result deviates about ten percent from the MFA-estimate quoted in Sec. III. We emphasize that this way to determine β is prone to systematic errors which have not been taken into account in the above error estimate. Moreover, we expect that our approach to fit β systematically produces too small a value because the curve of $\langle\hat{\Phi}\rangle$ will always be a smooth one when computed on a finite lattice.

[13]Because of the pole at $\Phi = 0$ such an expansion will only be valid in a sufficiently small vicinity of the respective minimum.

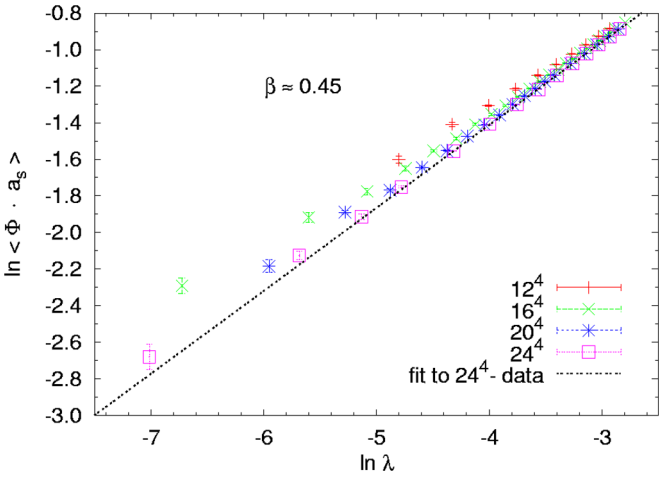

FIG. 8 (color online). Double logarithmic plot of $\langle\hat{\Phi}\rangle$ vs λ.

We conclude this section by presenting the Binder cumulant for the zero temperature case (i. e. $\gamma_{\text{aniso}} = 1$) in Fig. 9. The Binder cumulant [22] is defined as

$$U(L, \hat{\Lambda}) := 1 - \frac{1}{3}\frac{\langle|\hat{\Phi}|^4\rangle}{\langle|\hat{\Phi}|^2\rangle^2}. \tag{33}$$

In Fig. 9 the curves intersect at $\hat{\Lambda}_C \simeq 0.33$, which is in reasonable agreement both with the finite-size scaling result quoted in Table V and the mean-field estimate in Eq. (15). Furthermore, the numerical value of the Binder cumulant at the critical point is characteristic for each universality class. In [23] it was found by analytical means that for the four-dimensional Ising model $\langle s^4\rangle/\langle s^2\rangle^2 = 2.188\ldots$ where s is the average magnetization per unit

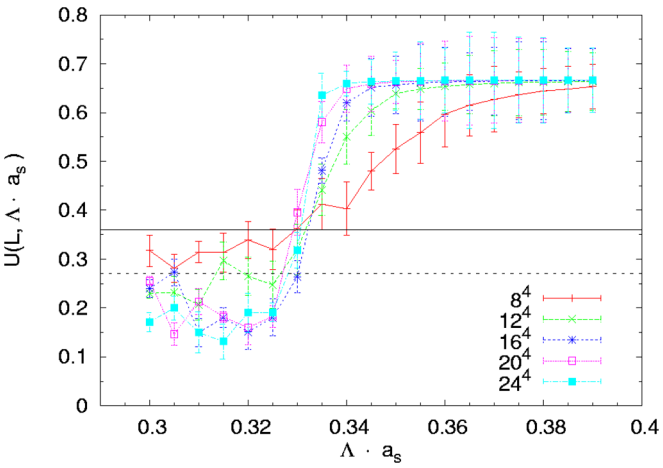

FIG. 9 (color online). The Binder cumulant $U(L, \hat{\Lambda})$ plotted vs $\hat{\Lambda}$ as computed on lattices of various sizes. The lines connecting the data merely serve to guide the eye. The dashed horizontal line corresponds to the result quoted in [23] while the solid line corresponds to the results of [24,25].

volume. Numerical studies of the four-dimensional Ising model [24,25] have yielded $\langle s^4\rangle/\langle s^2\rangle^2 = 1.92(3)$. The corresponding numerical values for the Binder cumulant $U(L, \hat{\Lambda}_C)$ as defined in Eq. (33) are 0.27 and 0.36 (independent of L, of course), respectively, and they are indicated in Fig. 9 by the solid and dashed line. It seems as if our data favors $\langle s^4\rangle/\langle s^2\rangle^2 = 1.92$. However, the data does not allow for a completely unambiguous discrimination against one of these two alternatives. Nevertheless, we infer that the findings for $U(L, \hat{\Lambda}_C)$ support the statement that the model at hand at zero temperature falls into the universality class of the 4-d Ising model.

V. SUMMARY AND CONCLUSIONS

In this work we have analyzed the theory governed by the Lagrangian (1) by both mean-field and Monte Carlo methods. At zero temperature, the mean-field analysis predicts the existence of a continuous phase transition and the universality class of the four-dimensional Ising model. Both results are in agreement with the Monte Carlo results. It seems that the additional symmetry of the potential $V(\Phi) = V(\Phi^*)$ does not have any impact on the critical behavior of the system.

Apart from the phase structure, we have also determined the mass gap of the theory both at zero and finite temperature. We found that its value is almost independent of temperature. The physical anisotropy did not show deviations from the bare coupling anisotropy γ within the margin of error. Finally, we obtained the critical exponents for the transition when varying Λ also at nonzero temperature from a finite-size scaling analysis. In the high temperature limit, the numerical values seem to indicate dimensional reduction to the three-dimensional Ising model. However, more work is necessary to understand the situation at high temperature.

ACKNOWLEDGMENTS

The numerical computations were carried out on the Fujitsu VPP5000 of the Rechenzentrum Karlsruhe and on the PC cluster at the Institute for Theoretical Physics of the University of Heidelberg. Computing support by Werner Wetzel is gratefully acknowledged.

APPENDIX

1. Some formulae for the MFA

In this appendix we summarize some technical details of the mean-field approximation presented in Sec. III. We use $\gamma = 1$. It is straightforward to extend the analysis to $\gamma > 1$, however, only for γ less than about 2 are the results, at least qualitatively, reasonable, for larger anisotropy a more involved analysis would be necessary.

We start by noting that the functions $F_n(\hat{\Lambda}, m)$ defined in Eq. (12) admit the following series expansion in m:

$$F_n(\hat{\Lambda}, m) = (2d)^n \sum_{k=0}^{\infty} \frac{1}{k!}(2dm)^k \times \int_0^{\infty} dR R^{n+k+1} e^{-\tilde{V}(R)} \times \int_0^{2\pi} d\Theta (\cos\Theta)^{n+k} e^{\hat{\Lambda}^4 \cos(2\Theta)}. \quad \text{(A1)}$$

Note that the terms with odd $n + k$ vanish by virtue of the symmetry properties of the Θ-integral. From this expression we can obtain the derivatives at $m = 0$, to be used in (14) and (17), in terms of the integrals:

$$R_n(\hat{\Lambda}) = \frac{1}{4}\int_0^{\infty} dR R^{2n+1} e^{-\tilde{V}(R)} = 2\left(\frac{\hat{\Lambda}^6}{2d + \hat{\Lambda}^2}\right)^{(n+1)/2} K_{n+1}(\hat{\Lambda}^3\sqrt{2d + \hat{\Lambda}^2}) \quad \text{(A2)}$$

$$T_n(\hat{\Lambda}) = \frac{1}{4}\int_0^{2\pi} d\Theta (\cos^2\Theta)^n e^{\hat{\Lambda}^4 \cos(2\Theta)} = \frac{\pi}{2^{n+1}} \sum_{k=0}^{n} \binom{n}{k} \frac{\partial^k}{\partial u^k} \mathrm{I}_0(u)|_{u=\hat{\Lambda}^4}. \quad \text{(A3)}$$

The $\omega = \frac{\pi}{2}$ solution can be obtained by reversing the sign of the $\cos(2\Theta)$ term in (A1).

2. Implementation of the cluster algorithm

This appendix describes our implementation of a cluster algorithm for the model. We start by rewriting the lattice action equation (3) in terms of the real and imaginary parts $\hat{x}_n$ and $\hat{y}_n$ of each field variable $\hat{\Phi}_n$, which yields

$$S[\hat{\Phi}] = \frac{1}{2\gamma}\sum_n \Big\{ -\gamma^2 2(\hat{x}_n\hat{x}_{n+\hat{\tau}} + \hat{y}_n\hat{y}_{n+\hat{\tau}}) - 2\sum_j [\hat{x}_n\hat{x}_{n+\hat{j}} + \hat{y}_n\hat{y}_{n+\hat{j}}] + 2(3+\gamma^2)|\hat{\Phi}_n|^2 + V(\hat{\Phi}_n)\Big\}.$$

We now identify a set of Ising-like degrees of freedom in the model by defining $s_n := \mathrm{sign}(\hat{x}_n) = \mathrm{sign}(\mathrm{Re}\hat{\Phi}_n)$ which we will use to set up the cluster algorithm. The action can then be rewritten as $S = S_{\mathrm{Ising}} + S_{\mathrm{Rest}}$ where S_{Rest} does not depend on the $\{s_n\}_n$ and

$$S_{\mathrm{Ising}}[\hat{\Phi}] = -\sum_n \Big\{ \gamma|\hat{x}_n||\hat{x}_{n+\hat{\tau}}|s_n s_{n+\hat{\tau}} + \sum_j \Big(\frac{1}{\gamma}|\hat{x}_n||\hat{x}_{n+\hat{j}}|s_n s_{n+\hat{j}}\Big)\Big\} = -\sum_n\sum_\mu J_{n,n+\hat{\mu}} s_n s_{n+\hat{\mu}} = -\frac{1}{2}\sum_{\langle l,n\rangle} J_{l,n} s_l s_n. \quad \text{(A4)}$$

Here we have defined a set of site-dependent nearest neighbor couplings as

$$J_{l,n} := \begin{cases} \gamma|\hat{x}_l||\hat{x}_n| & \text{if l, n are timelike neighbors} \\ \frac{1}{\gamma}|\hat{x}_l||\hat{x}_n| & \text{if l, n are spacelike neighbors.} \end{cases} \tag{A5}$$

We have chosen to embed Ising spins only in the real part of the field. Because of the shape of the potential we expect the imaginary part to be less affected by critical slowing down, if at all. Moreover, we note that it is not possible to define Ising spins from a projection on a random axis in the complex $\hat{\Phi}_n$-plane as it can be done for instance in the case of the XY-model. The reason for this is that the potential does not possess the necessary symmetry; it is in general not possible to flip the projection of $\hat{\Phi}_n$ on an arbitrary axis without altering the value of S_{Rest}. It remains to set up a cluster algorithm for the Ising- like degrees of freedom. The dynamics of the spin variables $\{s_n\}_n$ is equivalent to the one of a four-dimensional Ising model governed by the Hamiltonian

$$H_{\text{Ising}} \equiv S_{\text{Ising}} = -\frac{1}{2}\sum_{\langle l,n\rangle} J_{l,n} s_l s_n. \tag{A6}$$

We then proceed in the standard way [26–28] by introducing bond variables $d_{l,n}$ for all pairs of nearest neighbors l, n. From the literature (cf. e.g. [27]) it is known that the probability for a bond to be active has to be chosen as

$$p_{\text{act}}(d_{l,n}) = \begin{cases} 0 & \text{if } s_l \neq s_n \\ 1 - \exp(-2J_{l,n}) & \text{if } s_l = s_n \end{cases} \tag{A7}$$

in order to implement the correct dynamics for the Ising Hamiltonian (A6). After activating each bond variable with this probability we proceed as described in [28]: First, we choose a lattice site at random. Then we track the percolation cluster to which this site belongs and flip the real parts $\hat{x}_n \mapsto -\hat{x}_n$ of all field variables in the percolation cluster.

[1] M. E. Fisher, Rev. Mod. Phys. **70**, 653 (1998).
[2] R. Hofmann, Int. J. Mod. Phys. A **20**, 4123 (2005); **21**, 6515(E) (2006).R. Hofmann, Mod. Phys. Lett. A **21**, 999 (2006); **21**, 3049(E) (2006).
[3] R. Hofmann, arXiv:hep-th/0508212.
[4] R. Hofmann, Mod. Phys. Lett. A **22**, 2657 (2007).
[5] J. Engels, F. Karsch, and H. Satz, Nucl. Phys. **B205**, 239 (1982).
[6] G. Burgers, F. Karsch, A. Nakamura, and I. O. Stamatescu, Nucl. Phys. **B304**, 587 (1988).
[7] H. E. Stanley, *Introduction to Phase Transitions and Critical Phenomena* (Clarendon Press, Oxford, 1971).
[8] N. Metropolis *et al.*, J. Chem. Phys. **21**, 1087 (1953).
[9] M. Creutz *et al.*, Phys. Rep. **95**, 201 (1983).
[10] R. C. Brower and P. Tamayo, Phys. Rev. Lett. **62**, 1087 (1989).
[11] A. D. Sokal, Nucl. Phys. B, Proc. Suppl. **20**, 55 (1991).
[12] A. L. Talapov and H. W. J. Blöthe, J. Phys. A **29**, 5727 (1996).
[13] M. Schiestl, Ph.D. thesis, Universität Heidelberg, 1991.
[14] J. C. Le Guillou and J. Zinn-Justin, Phys. Rev. B **21**, 3976 (1980).
[15] L. von Löhneysen, R. E. Shrock, and I. O. Stamatescu, Phys. Lett. B **205**, 321 (1988).
[16] D. O'Connor and C. R. Stephens, J. Phys. A **25**, 101 (1992).
[17] D. O'Connor and C. R. Stephens, Nucl. Phys. **B360**, 297 (1991).
[18] S.-B. Liao and M. Strickland, Nucl. Phys. **B497**, 611 (1997).
[19] M. E. Fisher and A. Nihat Berker, Phys. Rev. B **26**, 2507 (1982).
[20] J. L. Cardy and P. Nightingale, Phys. Rev. B **27**, 4256 (1983).
[21] K. Binder and D. P. Landau, Phys. Rev. B **30**, 1477 (1984).
[22] K. Binder, Phys. Rev. Lett. **47**, 693 (1981).
[23] E. Brézin and J. Zinn-Justin, Nucl. Phys. **B257**, 867 (1985).
[24] P.-Y. Lai and K. K. Mon, Phys. Rev. B **41**, 9257 (1990).
[25] N. Aktekin, J. Stat. Phys. **104**, 1397 (2001).
[26] C. M. Fortuin and P. W. Kasteleyn, Physica (Utrecht) **57**, 536 (1972).
[27] R. H. Swendsen and J. S. Wang, Phys. Rev. Lett. **58**, 86 (1987).
[28] U. Wolff, Phys. Rev. Lett. **62**, 361 (1989).